RSC Advances

ROYAL SOCIETY OF CHEMISTRY

www.rsc.org/advances

Synthesis of {110}-faceted rutile TiO_2 nanocrystals from tetratitanate nanoribbons for improving dye-sensitized solar cell performances.

Yi-en Du,[a,b] Jun Li,[a] Yufang Liu,*[a] Xianjun Niu,[a] Fang Guo,[a] and Qi Feng[b]

[a] School of Chemistry & Chemical Engineering, Jinzhong University, Jinzhong, Shanxi, 030619, P. R. China. E-mail: sxyclyf@sina.com.

[b]Department of Advanced Materials Science, Faculty of Engineering, Kagawa University, 2217-20 Hayashi-cho, Takamatsu-shi, 761-0396, Japan.

ABSTRACT {110}-faceted rutile TiO_2 nanocrystals with nanorods and nanoflowers morphologies were synthesized through simple hydrothermal treatment of a tetratitanate nanoribbons precursor. The nanostructures and the formation reaction mechanism of the rutile TiO_2 nanocrystals from the layered tetratitanate nanoribbons were investigated using X-ray diffraction (XRD), field emission scanning electron microscopy (FE-SEM), transmission electron microscope (TEM) and selected-area electron diffraction (SAED). The transformation from the layered phase into the rutile TiO_2 may experience several stages during the hydrothermal reaction including dissolution of nanoribbons, recrystallization of $[Ti(OH)_6]^{2-}$ octahedral fragments, and part dissolution and aggregation of the rutile TiO_2 nanorods. Furthermore, the dye-sensitized solar cell (DSSC) performance of the synthesized rutile nanocrystals was also characterized, which showed a superior photovoltaic performance, compared to the benchmark P25 TiO_2.

Introduction

Design and synthesis of titanium dioxide (TiO_2) nanostructures with different morphologies and exposed specific facets have attracted considerable attention over the past decade, not only because of their considerable applications in photocatalysis,[1,2] dye-sensitized solar cells (DSSCs),[3,4] gas sensors[5], lithium-ion batteries,[6] etc; but also because of their thermal and chemical stability, relatively high photocatalytic activity, nontoxicity, and cost effectiveness.[7] In nature, TiO_2 mainly exists in four crystalline phases: anatase (tetragonal, space group $I4_1/amd$), rutile (tetragonal, space group $P4_2/mmm$), brookite (orthorhombic, space group *Pbca*), and

TiO_2 (B) (monoclinic, space group C_2/m).[8] Among the four crystalline forms, anatase TiO_2 with specific active facets exposed has attracted enormous attention for its superior photocatalytic properties and excellent photovoltaic performances.[9,10,11]The average surface energies of anatase TiO_2 increase in the order of {101} facet (0.44 J/m^2) <{100} facet (0.53 J/m^2) <{001} facet (0.90 J/m^2).[12] Since the crystal facets of rutile ({011} and {110} facets) and anatase ({001} and {011} facets) TiO_2 particles and their roles in photocatalytic reactions were first reported by Ohno *et al.*,[13] the morphologies and crystals facet-controlled synthesis of TiO_2 have been extensively investigated to improve their photocatalytic properties and photovoltaic performances. For instance, anatase TiO_2 nanocrystals with exposed {010} facets and controllable morphologies were firstly synthesized by hydrothermal treatment of the $[Ti_{1.73}O_4]^{1.07-}$ nanosheets. They exhibited higher photocatalytic activity than the normal spherical nanocrystals without a specific facet on the surface.[14] After that, anatase TiO_2 single crystals with a large percentage of {001} facets were synthesized by using hydrofluoric acid solution as a capping agent.[15] Using organic morphology controlling agents, rhombic-shaped anatase TiO_2 nanocrystals and tetragonal faceted-nanorods with exposed {010} facets were prepared, and they exhibited conspicuous photocatalytic activity and improved photovoltaic conversion efficiency, respectively.[16,17] Recently, the anatase nanocrystals with a large percentage of {010} facets and [111]-facets were prepared by hydrothermal treatment of titanate nanosheets precursors. They exhibited higher photocatalytic than the commercial P25 sample.[18,19]

Compared with anatase TiO_2, relatively few researches have been reported on rutile TiO_2. Feng *et al*. firstly reported the fabrication of dye-sensitized solar cells from vertically oriented single crystalline rutile TiO_2 nanowires arrays on transparent conducting fluorine-doped tin oxide (FTO) glass substrates.[20] After that, Sun *et al.* reported that rutile nanowires grown on a titanate nanosheet film performed better in dye-sensitized solar cells than those on bare FTO conducting glass in terms of all cell parameters.[21] Liu *et al.* reported a facile one-pot hydrothermal synthesis of pure rutile TiO_2 photoanode with 100% exposed pyramid-shaped {111} surfaces on a FTO

conducting substrate.[22] Recently, hierarchical double-layered TiO_2 flower-rod structure composed of three-dimensional (3D) TiO_2 nanoflowers and one-dimensional (1D) nanorods on FTO conducting glass were synthesized by hydrothermal method.[23,24] As shown above, the rutile crystals are usually prepared in FTO conducting glass substrates, which are relatively difficult in the process of experimental operation.

Herein, we report a facile precursor route to prepare rutile TiO_2 nanorods and nanoflowers with exposed {110} facets using a layered tetratitanate as a start material. Through ion-exchange, exfoliation, and hydrothermal treatment, the layered tetratitanate precursor was converted into the desired rutile TiO_2 material. The possible transformation mechanism of the rutile TiO_2 nanocrystals and the photovoltaic performance were investigated. And the photovoltaic performance was compared with the benchmark P25 TiO_2 (commercial TiO_2 power, ~87% anatase and ~13% rutile).

Methods

Regents and materials

Potassium tetratitanate ($K_2Ti_4O_9$) was obtained from Otsuka Chemical Co., Ltd. Tetramethylammonium hydroxide solution (TMAOH, 15%) and hydrochloric acid (HCl, 35.0-37.0%) were purchased from Wako Pure Chemical Industries, Ltd. Cis - di (thiocyanate) bis (2,2′-bipyridyl - 4,4′ - dicarboxylate) - ruthenium (II) bis - tetrabutylammonium (N719) was purchased from Sigma-Aldrich. Degussa P25 was obtained from Nippon Aerosil, Ltd. All the chemicals and reagents were of analytical grade and were used as received without further purification. Deionized water was obtained from Milli-Q ultra-pure system (Yamata Scientific Co., Ltd.).

Preparation of layered tetratitanate nanoribbon colloidal solutions

The layered tetratitanate nanoribbon colloidal solutions were prepared from layered tetratitanate $K_2Ti_4O_9$ (KTO). The KTO sample (10.0 g) was acid treated with 1 mol/L HCl solution (1 L) for 3 days under stirring conditions to exchange K^+ ions with H^+ to obtain a protonic tetratitanate $H_2Ti_4O_9 \cdot 0.25H_2O$ (HTO), or written as

$(H_2O)_{0.25}Ti_4O_7(OH)_2$.[25] The acid solution was replaced daily with a fresh one in order to remove K^+ completely from the compounds. The HTO layered tetratitanate was washed with copious Milli-Q water to remove excess acid and dried using a freeze drier. 3.0 g of the HTO sample was hydrothermally treated in a 12.5% TMAOH solution (30 mL) at 100 °C for 24 h under stirring to intercalate TMA^+ ions into the interlayer and to obtain TMA^+-intercalated HTO sample. And further, the obtained sample was dispersed in 300 mL of Milli-Q water at room temperature by stirring for 24 h to exfoliate the TMA^+-intercalated HTO sample to its nanoribbons. After removal of the nonexfoliated particles by filtration, the tetratitanate nanoribbon colloidal solution was obtained.

Preparation of TiO_2 nanorods-nanoflower from layered tetratitanate nanoribbon colloidal solution

TiO_2 nanoparticles were prepared by hydrothermal treatment of the tetratitanate nanoribbon colloidal solution after adjusting pH value to 1.0 with a 3 mol/L HCl solution. 40 mL of the pH adjusted colloidal solution was sealed in a Teflon-lined stainless steel autoclave with a capacity of 70 mL at 120 °C and 140 °C for 24 h, respectively. After the hydrothermal treatment, the sample was separated from the solution by centrifugation, followed by washing several times with Milli-Q water, and finally dried using a freeze drier. The obtained TiO_2 sample was designated as pH1.0-T*x*, where *x* is the desired temperature of the hydrothermal treatment.

Fabrication of dye-sensitized solar cell.

A paste of rutile TiO_2 nanorods-nanoflowers was prepared by mixing of 0.5 g of the TiO_2 nanocrystals sample, 2.5 g of ethanol, 2.0 g of α-Terpineol, 1.4 g of 10 wt% solution of Wako-ethyl-cellulose 10 (8-14 mPas), and 1.1 g of 10 wt% solutions of Wako-ethyl-cellulose 45 (45-65mPas). The mixture was dispersed by ultrasonic treatment for 5 minutes, followed by ball-milling for 3 days at room temperature. After ball-milling, a sticky paste was obtained by using a rotary evaporator to remove the ethanol. The DSSCs were fabricated by the following steps: (i) preparation of photoelectrodes, (ii) dye adsorption of photoelectrodes, and (iii) assembly. For prepare the photoelectrodes, the fluorine-doped tin oxide (FTO) conducting glass

plates (12.5 × 12.5 mm) were cleaned for 5 min with Milli-Q water and alcohol, respectively, using an ultrasonic bath, in order. The FTO glass plate was immersed in 0.1 M titanium tetraisopropoxide (TTIP) solution for several seconds, and then sintered at 480 °C in muffle furnace for 60 min to coat the FTO glass surface with a dense TiO_2 thin film. The prepared TiO_2 paste was coated on the TTIP-treated FTO glass plate by a doctor-blade technique. The films thickness was controlled by thickness of the adhesive tape used as the spacer. After being coated with the paste on the FTO glass plate, the doctor-bladed FTO glass plate was calcined at 315 ^oC for 15 min. Do such working several times to obtain a thickness of TiO_2 films around 14 μm, and then calcined it at 450 ^oC for 30 min. We also prepared similar films from the commercially available Degussa P25 TiO_2 for comparison. The TiO_2 films were treated with 0.1 M TTIP solution as described above, and then calcined at 480 ^oC for 60 min to obtain TiO_2 porous electrode. For the dye adsorption, the sintered TiO_2 porous electrode was soaked in 3×10^{-4} mol/L N719 dye solution in a 1:1 acetonitrile (super dehydrated) - tert-butyl alcohol for 24 h at room temperature and washed with absolute ethanol for removing the unadsorbed dyes. The DSSC was comprised of the dye-sensitized TiO_2 electrode and a Pt-counter electrode with an electrolyte solution between the electrodes. The electrolyte consisting of 0.60 mol/L 1-butyl-3-methylimidazolium iodide, 0.03 mol/L Iodine, 0.10 mol/L guanidine thiocyanate, and 0.50 mol/L 4-tert-butylpyridine in acetonitrile/valeronitrile (85:15, v/v), was injected into the cell through the edges between the two electrodes.

Characterization. The powder XRD measurements were performed on each sample by using a SHIMADZU XRD-6100 diffractometer with Cu Kα radiation, λ = 0.15406 nm, operated at 30 mA current and with a voltage of 40 kV. Field emission scanning electron microscopy (FE-SEM) was performed using a HITACHI S-90X machine at an operating voltage of 15 kV and current of 10 mA. Transmission electron microscope (TEM), high-resolution TEM (HR-TEM) and selected-area electron diffraction (SAED) were done with the JEOL (JEM-3010) machine at an operating voltage of 200 kV. The Brunauer-Emmett-Teller (BET) surface areas of the samples were determined by a TriStar II 3020 volumetric adsorption analyzer at -196 °C after

the samples were degassed at 120 °C for 5 h under high vacuum before the measurements. The photocurrent-voltage characteristic curves for the DSSCs were measured using a Hokuto-Denko BAS100B electrochemical analyzer under irradiation with simulated sunlight of AM 1.5 (100mW/cm^2), using a sunlight simulator (YSS-E40, Yamashita Denso) and a 0.25 cm^2 mask. The thicknesses of the TiO_2 films were measured using a SURFCOM 480A surface-shape determiner.

Results and discussion

Structure and morphology

The precursor, monoclinic KTO, is confirmed by a powder XRD pattern (JCPDS No. 32-0861, a = 18.25, b = 3.79, c = 12.01 Å, and β = 106.4°), as shown in Fig. 1(a). After the K^+/H^+ ion-exchange reaction, the basal spacing was changed from 8.68 Å for KTO to 7.78 Å for HTO (JCPDS No. 38-0700, a = 16.20, b = 3.74, c = 12.09 Å, and β = 105.7°), indicating the HTO sample maintains the same essential layered structure (Fig. 1(b)). To exfoliate the layered structure HTO into its nanoribbons, the HTO sample was hydrothermally treated in a TMAOH solution at 100 °C to intercalate TMA^+ ions into the interlayer. After the hydrothermal treatment, the TMA^+-intercalated tetratitanate sample still maintains the same layered structure, which shows the main diffraction peaks of (200), (400), and (600) with d-values of 18.02, 9.01, and 6.10 Å, respectively (Fig. 1(c)). The basal spacing was changed from 7.78 Å for HTO to 18.02 Å for TMA^+-intercalated tetratitanate, indicating that the TMA^+ ions were successfully intercalated into the interlayer space by H^+/TMA^+ ion-exchange. In view of the height of TMA^+ ion being 5.30 Å,[26] and the thickness of crystallographic nanoribbon being 5.70 Å,[27,28] the large basal spacing implies that the TMA^+-intercalated sample in its wet state contains double layers of the TMA^+ ions (2 × 5.30 + 5.70 = 16.30 Å) in the interlayer. The interlayer gallery height is a little higher than double layers of the TMA^+ ions might be caused by the presence of interlayer water.[29] When the TMA^+-intercalated tetratitanate is dispersed in a certain amount of Milli-Q water, the layered structure is exfoliated into nanoribbons, resulting in a tetratitanate nanoribbon colloidal solution.

As shown in Fig. 2(a), the HTO has a layer structure, and one layer consists of

linear groups of four [TiO_6] octahedrons with overlapping edges.[30] Fig. 2(b-d) show the typical FE-SEM images of KTO, HTO, and the exfoliated tetratitanate nanoribbons sample, respectively. The KTO sample exhibits a fibrous morphology, with a size of ~120-250 nm in width and several micrometers in length [Fig. 2(b)]. After the ion-exchange reaction, the HTO sample retaining the profile of the KTO [Fig. 2(c)], and the axis-direction of the HTO corresponds to the *b*-axis direction of the crystal [Fig. 2(e, f)]. The HR-TEM image [Fig. 2(g)] shows that the lattice spacing of 3.47 Å (lattice fringes perpendicular to the length of the nanoribbon) and 2.72 Å (lattice fringes parallel to the length of the nanoribbon), corresponding to the (010) and (004) facets of the HTO, respectively, revealing that the nanoribbon direction is in the [010]-direction.

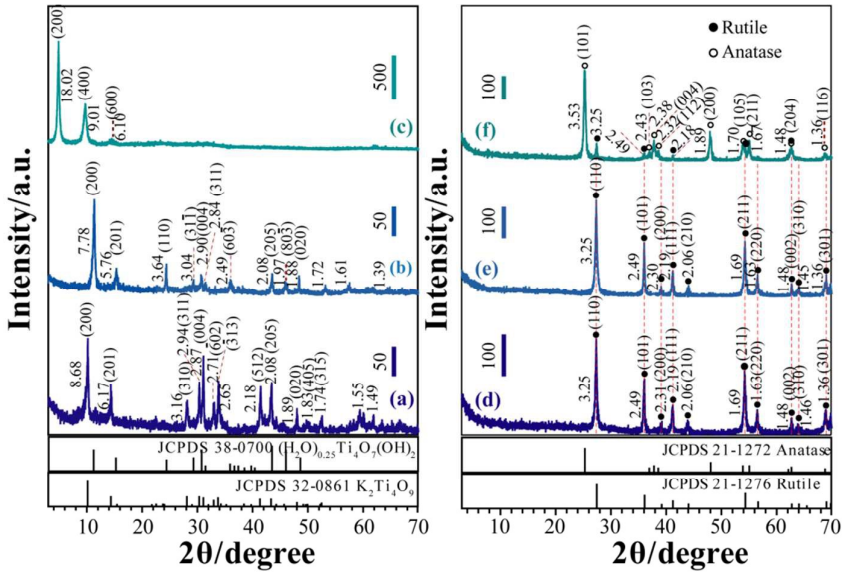

Fig. 1 XRD patterns of (a) $K_2Ti_4O_9$ (KTO), (b) $H_2Ti_4O_9 \cdot 0.25H_2O$ (HTO), (c) TMA^+-intercalated tetratitanate sample, (d) pH1.0-T120, (e) pH1.0-T140, and (f) P25 samples.

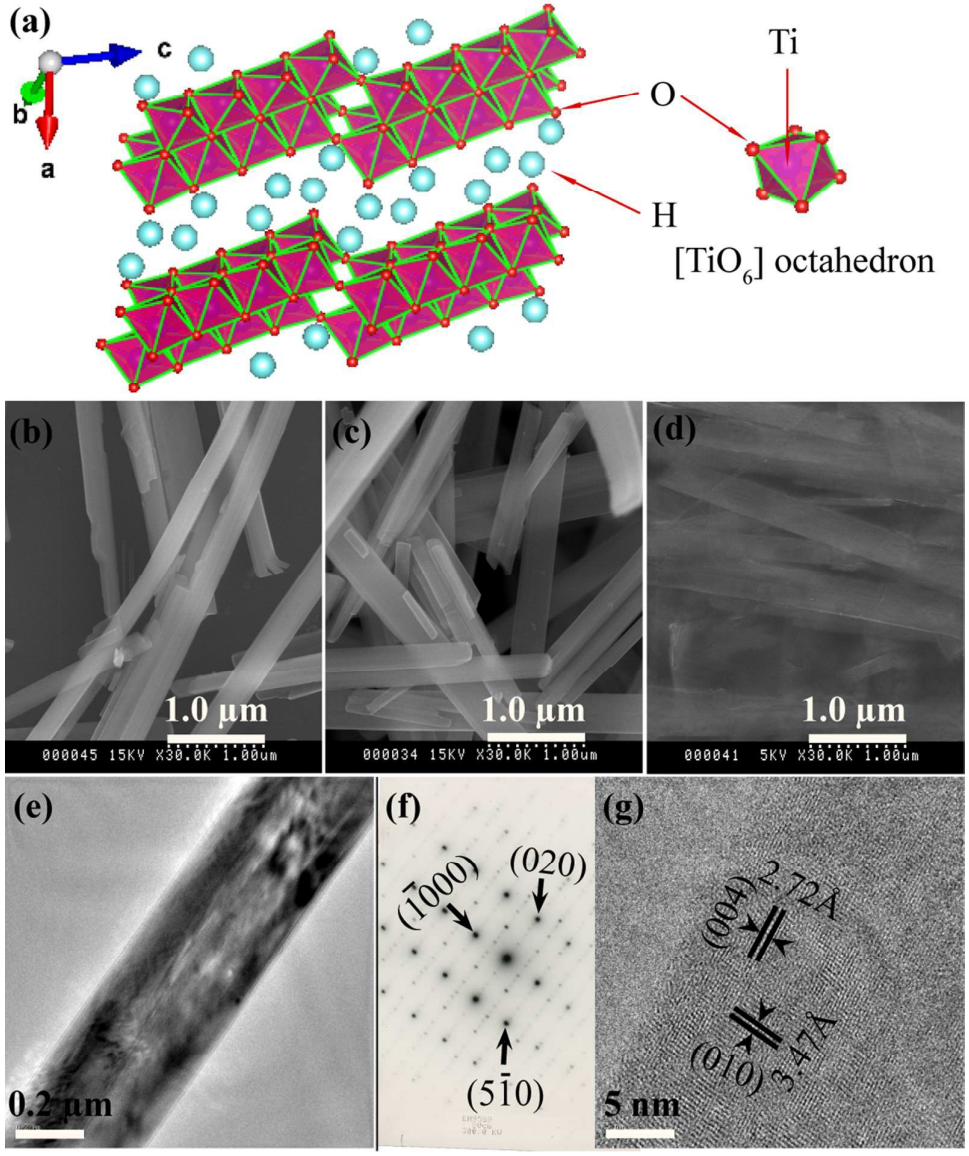

Fig. 2 (a) Crystal structure of $H_2Ti_4O_9 \cdot 0.25H_2O$ (HTO), FE-SEM images of (b) $K_2Ti_4O_9$ (KTO) sample, (c) $H_2Ti_4O_9 \cdot 0.25H_2O$ (HTO) sample, and (d) the exfoliated tetratitanate nanoribbons sample, TEM image and SAED pattern of (e, f) $H_2Ti_4O_9 \cdot 0.25H_2O$ (HTO) sample, and HR-TEM image of (g) an exfoliated tetratitanate nanoribbon sample.

The XRD patterns of the samples prepared by hydrothermal treatment of the tetratitanate nanoribbon colloidal solution at pH 1.0 at 120 and 140 °C, are shown Fig. 1(d, e), respectively. The positions of the diffraction peaks indicate that both the samples are rutile type of TiO_2 (JCPDS No. 21-1276, tetragonal system, $a = b = 4.59$ Å, $c = 2.96$ Å). And no anatase diffraction peaks are observed. As shown in Fig. 1(d, e), the diffraction peaks of rutile TiO_2 became stronger and sharper with the increase

of temperature, implying an increase of crystallinity. As shown in Fig. 1(f), the commercial P25 TiO_2 sample containing 87% anatase phase and 13% rutile phase, calculated from the integrated intensities of anatase (101), and rutile (110) peaks according to literature.[31,32]

Typically, FE-SEM images (Fig. 3(a-d)) show that the synthesized rutile TiO_2 samples are consisted of uniformed nanorods (with a size of ~1 μm in length and ~120 nm in width). Partial dissolution and reaggregation of these nanorods lead to some nanoflowers structure. Actually, each nanorod is consisting of hundreds of highly ordered ultrafine rutile nanowires (with a size of ~8 nm in width), which is confirmed by HR-TEM image shown in Fig. 3(e, f). The lattice fringe has *d*-spacing values of 3.25 and 2.95 Å, corresponding to (110) and (001) planes of rutile TiO_2, respectively, and the angle between the two planes is 90°, which is identical to the theoretical value between the (110) and (001). Fig. 3f also reveals that the rodlike crystal facets are parallel to {110} facets, and the elongation of the crystal is parallel to <001> direction. That is, the long axis of the rodlike crystal corresponds to *c*-axis direction of the rutile structure and exposed crystal facets are {110} facets.[33]

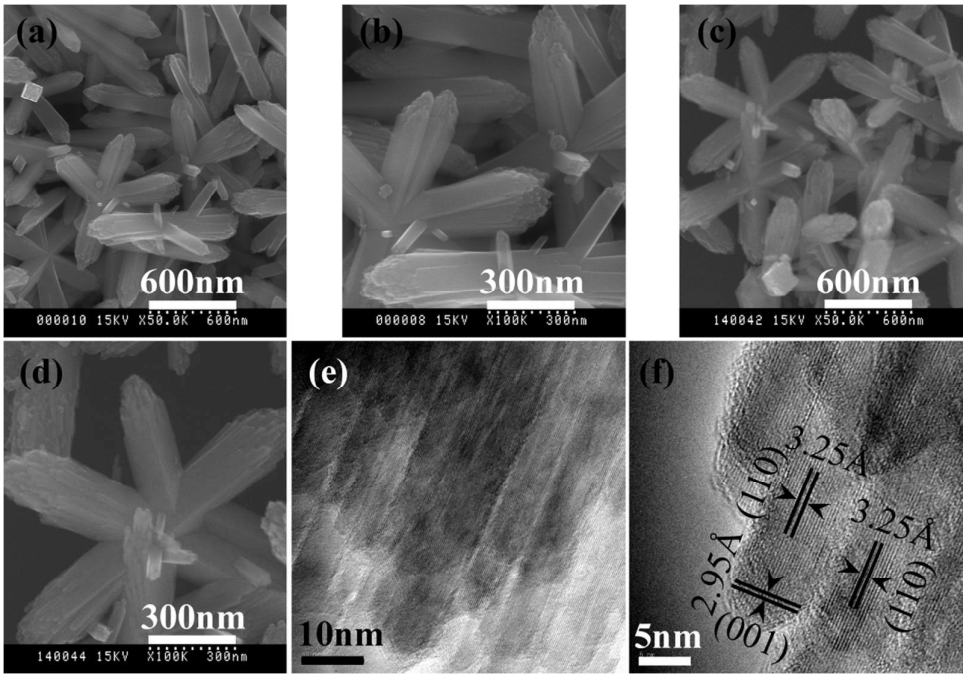

Fig. 3 FE-SEM images of (a, b) pH1.0-T120, and (c, d) pH1.0-T140 sample; TEM and HR-TEM images of (e, f) pH1.0-T120 sample.

Transformation reaction mechanism from tetratitanate nanoribbons to nanorods-nanoflowers of rutile TiO_2

On the basis of the above results, we proposed a possible reaction mechanism for the formation of nanorods-nanoflowers of rutile TiO_2 from tetratitanate nanoribbons in the hydrothermal reaction process, which is illustrated in Fig. 4. In this process, first the TMA^+-intercalated layered tetratitanate structure is exfoliated into elementary host $[Ti_4O_9]^{2-}$ nanoribbons. The cations of TMA^+ and H_3O^+ locate on the surface of $[Ti_4O_9]^{2-}$ nanoribbons to balance the negative charge. The formation of the nanorods-nanoflowers of rutile TiO_2 architecture from the $[Ti_4O_9]^{2-}$ nanoribbons may experience several stages during the hydrothermal reaction including dissolution of nanoribbons, recrystallization of $[Ti(OH)_6]^{2-}$ octahedral fragments, and part dissolution and aggregation of the nanorods. Initially the $[Ti_4O_9]^{2-}$ nanoribbons are split to small, primarily $[Ti(OH)_6]^{2-}$ octahedral monomers along the corner-shared and edge-shared oxygen atoms in high acidic conditions. Subsequently, the rutile TiO_2 nanorods are formed by sharing equatorial edges of the $[Ti(OH)_6]^{2-}$ octahedral monomers. Finally, the rutile TiO_2 nanorods occurred partly dissolution and aggregated to nanoflowers. The transformation of $[Ti_4O_9]^{2-}$ nanoribbons to rutile TiO_2 can be described as follows.

$$[Ti_4O_9]^{2-} + 15H_2O = 4[Ti(OH)_6]^{2-} + 6H^+ \quad (1)$$

$$[Ti(OH)_6]^{2-} + 2H^+ = TiO_2 + 4H_2O \quad (2)$$

The acid condition can slow down the dissolution reaction of $[Ti_4O_9]^{2-}$ by providing free H^+ as present in reaction (1), which is favorable to form the oriented 1D TiO_2 nanorod by dehydration reaction (i.e., oxolation) between OH ligands in $[Ti(OH)_6]^{2-}$ octahedral monomers (2). Meanwhile, Cl^- provided by HCl can preferentially adsorb on rutile TiO_2 (110) plane and postpone the growth rate of (110) plane, which is facilitative for the anisotropic growth of rutile nanorods along [001] direction.[23] With the proceeding of the hydrothermal reaction, dissolution of the rutile TiO_2 nanorods occurred partly, which are inclined to aggregate to form the core of the flowers. As the hydrothermal reaction further prolonging, these aggregated rutile TiO_2 nanorods would develop bigger, leading to the formation of rutile TiO_2 nanoflowers.

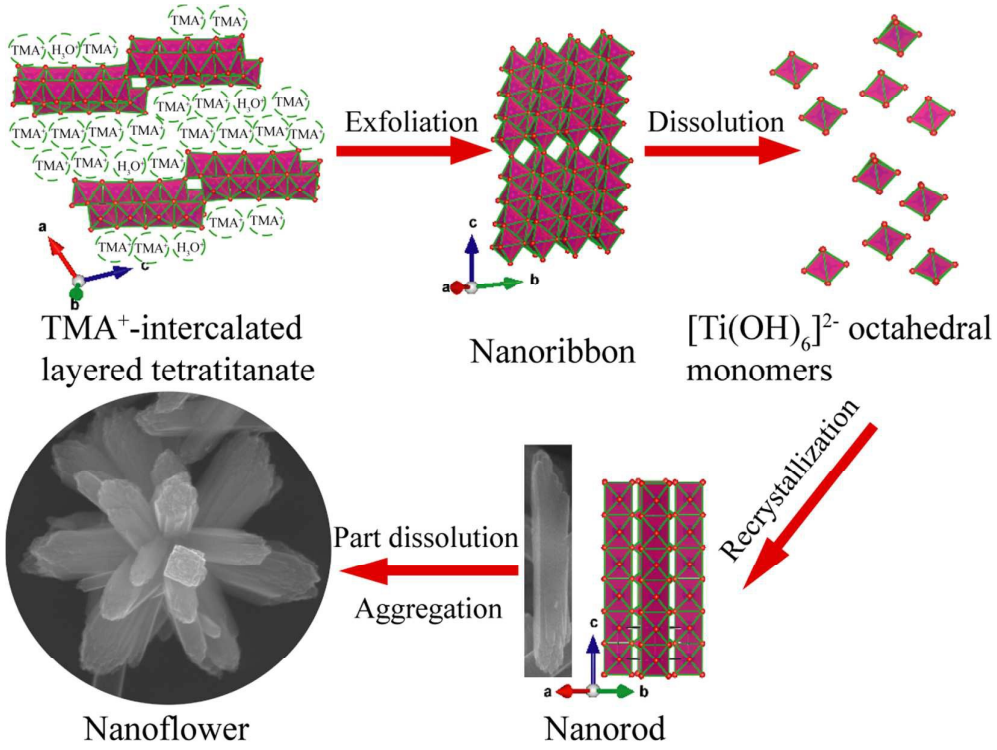

Fig. 4 Transformation reaction mechanism from TMA^+-intercalated layered tetratitanate to rutile TiO_2 nanorods-nanoflowers structure.

DSSC performance of TiO_2 nanocrystals

To study the DSSCs performance of the TiO_2 nanocrystals, we fabricate DSSCs using T120-pH1.0 and P25 TiO_2 nanocrystal samples. Fig. 5 depicts the photocurrent-voltage characteristics of two typical DSSCs assembled from the rutile nanorods-nanoflowers and P25 TiO_2, respectively, under AM 1.5 illumination (100 mW cm^{-2}). The corresponding photovoltaic performance parameters of the two DSSCs including short-circuit photocurrent density (J_{sc}), open circuit voltage (V_{oc}), fill factor (FF), and power conversion efficiency (η) are summarized in Table 1. The J_{sc}, V_{oc}, and η values of T120-pH1.0-based DSSC were improved by 28.2% (from 10.84 to 13.90 mA/cm^2), 5.0% (from 0.717 to 0.753 V), and 31.5% (from 3.91 to 5.14%), compared to P25-based DSSC, respectively. The higher η value of T120-pH1.0 than P25 TiO_2 is due to enhancements of the J_{sc} and V_{oc} values. The

higher performance of T120-pH1.0-based DSSC can be explained by the nanostructure and surface structure of T120-pH1.0 nanocrystals.

It is well know that the interfacial electron transfer influence on DSSCs efficiency. And the efficiency of the solar energy conversion process is closely related to the structure and stability of the dye-TiO_2 interface.[34] The dye-TiO_2 interface starts with the absorption of the sun energy, followed the excited electron from the dye is injected into the conduction band of the TiO_2.[35] Rutile TiO_2 nanorods-nanoflowers are composed of hundreds of ultrafine nanowires with the width of ~8 nm [Fig. 3(e, f)]. The V_{oc} value of T120-pH1.0-based DSSC was higher than that of P25 TiO_2 with the same film thickness. The nanowire architecture can help increase of the rate of charge transport as compared to P25 TiO_2 nanoparticles in the porous TiO_2 film because of lower concentration of grain boundaries.[36] The enhancement of porous TiO_2 film conductivity can suppress the charge recombination at interface between TiO_2 surface and I_3^- in the electrolyte. As the V_{oc} value of the DSSCs is determined by the differences between the quasi-Fermi level of TiO_2 and the redox potential of I^- and I_3^-, a lower electron-hole recombination rate results in a negative shift in the Fermi level of TiO_2, namely give a high V_{oc} value.[37]

The dye adsorption behavior on the TiO_2 nanocrystal surface has an important influence on the J_{sc} value of the DSSCs. The ultrafine nanowires arrays provide a larger BET surface area (79.6 m^2/g for T120-pH1.0) compare with the benchmark P25 TiO_2 (49.7 m^2/g), resulting in a larger dye adsorption amount than P25 TiO_2. The crystal facet on the TiO_2 surface can affect also the dye adsorption behavior. We have been reported that the N719 dye adsorption equilibrium constant (K_{ad}) on anatase nanocrystals surfaces increased in the order of non-specific surface < [111]-faceted surface < {010}-faceted surface, which corresponds to the increasing order of the J_{sc} value, namely, the strong binding between the dye and TiO_2 surface can enhance the J_{sc} value.[18] It has been reported that there is a stronger interaction between the dye molecule and the rutile TiO_2 {110} facets, which can improve the charge transfer rate

from the molecule to the TiO_2 surface.[34] The dye molecules may be anchored more strongly on {110}-faceted rutile nanocrystal surface of T120-pH1.0 than that on the anatase TiO_2 nanocrystal surface of P25, and the strong anchoring can facilitate the electron injection rate from the N719 dye molecules into the conduction band of TiO_2, resulting in the enhancement of the J_{sc}.[38]

For rutile TiO_2, the {110}, {100} and {001} facets have been studied, among them, the {110} facet is the most stable crystal surface.[39] The surface energy of the rutile TiO_2 {110} facet is 0.31 J/m^2, which contains two different kinds of titanium atoms (sixfold coordinated Ti atoms and fivefold coordinated Ti atoms) among the [001] direction.[39,40] The rutile TiO_2 {100} facets (fivefold coordinated Ti atoms) has received considerably less attention than the {110} facets, because it is difficult to determine conclusively the exact surface geometry.[39] The rutile TiO_2 {001} facet contains only fourfold coordinated Ti atoms and twofold coordinated O atoms.[39] Hence the number of broken bonds in the surface is higher the {110} and {100} surfaces. Consequently, the rutile {001} facet has a high surface energy. However, the {110} facets have both a favorable surface atomic structure and a surface electron structure for photocatalytic reactions, which make the reducing electrons in the conduction-band can be transferred via the surface fivefold coordinated Ti atoms as active reaction sites. And the efficient consumption of exited electrons in the photoreduction reactions can simultaneously promote the involvement of holes in photooxidation rections. Such a cooperative mechanism existing on {110} facets is responsible for its having the higher performance for photocatalytic reactions.[41] We think the surface atomic structures and charge transfer mechanisms of rutile facets would affect strongly also on the DSSCs performances.

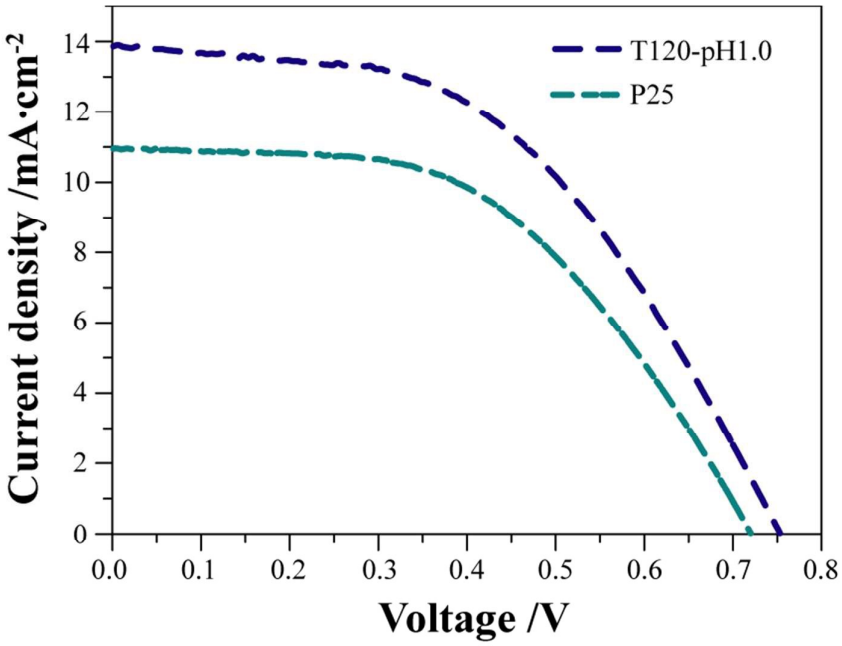

Fig. 5 Photocurrent-voltage characteristic curves of DSSCs fabricated using the nanocrystal samples of T120-pH1.0 rutile and P25.

Table 1 Summary of the device parameters under AM 1.5G irradiation.

Sample	Film thickness (μm)	J_{sc} (mA/cm^2)	V_{oc}(V)	FF(%)	η (%)
T120-pH1.0	13.5	13.90	0.753	49.1	5.14
P25	14.1	10.84	0.717	50.2	3.91

Conclusions

The {110}-faceted rutile TiO_2 nanocrystals composed of nanorods and nanoflowers can be synthesized by simple hydrothermal treatment of tetratitanate nanoribbons. The possible formation mechanism from the layered tetratitanate nanoribbons to the rutile TiO_2 may experience several stages, including dissolution of nanoribbons, recrystallization of $[Ti(OH)_6]^{2-}$ octahedral fragments, and part dissolution and aggregation of the rutile TiO_2 nanorods. The {110}-faceted rutile TiO_2 nanocrystals exhibited an excellent photovoltaic performance, compared to the benchmark P25 TiO_2, owing to the TiO_2 nanorods-nanoflowers composed of hundreds of ultrafine nanowires can enlarge the surface area for N719 dyes loading, accelerate the movement of photoelectrons and suppress the recombination of photogenerated

electrons and holes in the porous TiO_2 film. The surface atomic structure and electron structure of rutile can affect also on the DSSCs performances.

Notes

The authors declare no competing financial interest.

Acknowledgements

This work was supported part by Science and technology innovation project of Shanxi Province Education Department (Grant no. 20121026), the Grants-in-Acid for Doctor Research Funds from Jinzhong University and the Grants-in-Aid for Scientific Research (B) (no. 26289240) for the Promotion of Science.

References

1 N. Roy, Y. Sohn, and D. Pradhan, Sunergy of low-energy {101} and high-energy {001} TiO_2 crystal facets for enhanced photocatalysis, *ACS Nano*, 2013, **7**, 2532-2540.

2 C. H. Li, C. Koenigsmann, W. D. Ding, B. Rudshteyn, K. R. Yang, K. P. Regan, S. J. Konezny, V. S. Batista, G. W. Brudvig, C. A. Schmuttenmaer, and J.-H. Kim, Facet-dependent photoelectrochemical performance of TiO_2 nanostructures: an experimental and computational study, *J. Am. Chem. Soc.*, 2015, **137**, 1520-1529.

3 A. K. Patra, A. Dutta, and A. Bhaumik, Synthesis of cuboid-shaped single-crystalline TiO_2 nanocrystals with high-energy facets {001} and its dye-sensitized solar cell application, *J. Phys. Chem. C*, 2014, **118**, 16703-16709.

4 C. D. Chen, Y. Ikeuchi, L. F. Xu, G. A. Sewvandi, T. Kusunose, Y. Tanaka, S. Nakanishi, P. H. Wen, and Q. Feng, Synthesis of [111]- and {010}-faceted anatase TiO_2 nanocrystals from tri-titanate nanosheets and their photocatalytic and DSSC performances, *Nanosacle*, 2015, **7**, 7980-7981.

5 A. C. Parageorgiou, C. L. Pang, Q. Chen, and G. Thornton, Low-dimensional, reduced phases of ultrathin TiO_2, *ACS Nano*, 2007, **1**, 409-414.

6 S. H. Nam, H.-S. Shim, Y.-S. Kim, M. A. Dar, J. G. Kim, and W. B. Kim, Ag or Au nanoparticle-embedded one-dimensional composite TiO_2 nanofibers prepared via electrospinning for use in lithium-ion batteries, *ACS Appl. Mater. Interfaces*, 2010, **2**, 2046-2052.

7 C. Han, R. Luque, and D. D. Dionysion, Facile preparation of controllable size monodisperse anatase titania nanoparticles, *Chem. Commun*., 2012, **48**, 1860-1862.

8 W.-J. Ong, L.-L. Tan, S.-P. Chai, S.-T. Yong, and A. R. Mohamed, Highly reactive {001} facets of TiO_2-based composites: synthesis, formation, mechanism and characterization, *Nanoscale*, 2014, **6**, 1946-2008.

9 C. D. Chen, L. F. Xu, G. A. Sewvandi, T. Kusunose, Y. Tanaka, S. Nakanishi, and Q. Feng, Microwave-assisted topochemical conversion of layered titanate nanosheets to {010}-faceted anatase naocrystal for high performance photocatalysts and dye-sensitized solar cells, *Cryst. Growth Des*., 2014, **14**, 5801-5811.

10 D.-H. Wang, L. Jia, X.-L. Wu, L.-Q. Lu, and A.-W. Xu, One-step hydrothermal synthesis of N-doped TiO_2/C nanocomposites with high visible light photocatalytic activity, *Nanoscale*, 2012, **4**, 576-584.

11 Z. R. Wang, H. Wang, B. Liu, W. Z. Qiu, J. Zhang, S. H. Ran, H. T. Huang, J. Xu, H. W. Han, D. Chen, and G. Z. Shen, Transferable and flexible nanorod-assembled TiO_2 cloths for dye-sensitized solar cells, photodetectors, and photocatalysts, *ACS Nano*, 2011, **5**, 8412-8419.

12 M. Lazzeri, A. Vittadini, and A. Selloni, Structure and Energetics of Stoichiometric TiO_2 Anatase Surfaces, *Phys. Rev. B: Condens. Matter Mater. Phys*., 2001, **63**, 155409.

13 T. Ohno, K. Sarukawa, and M. Matsumura, Crystal facets of rutile and anatase TiO_2 particles and their roles in photocatalytic reactions, *New J. Chem*., 2002, **26**, 1167−1170.

14 P. H. Wen, H. Itoh, W. P. Tang, Q. Feng, Single nanocrystals of anatase-type TiO_2 prepared from layered titanate nanosheets: formation mechanism and characterization of surface properties, *Langmuir*, 2007, **23**, 11782-11790.

15 H. G. Yang, C. H. Sun, S. Z. Qiao, J. Zou, G. Liu, S. C. Smith, H. M. Cheng, and G. Q. Lu, Anatase TiO_2 single crystals with a large percentage of reactive facets, *Nature*, 2008, **453**, 638-642.

16 B. H. Wu, C. Y. Guo, N. F. Zheng, Z. X. Xie, and G. D. Stuky. Nonaqueous production of nanostructured anatase with high facets, *J. Am. Chem. Soc.*, 2008,

130, 17563-17567.

17 W. G. Yang, Y. L. Wang, and W. M. Shi, One-step synthesis of single-crystal anatase TiO_2 tetragonal faceted-nanorods for improved-performance dye-sensitized solar cells, *CrystEngComm*, 2012, **14**, 230-234.

18 Y.-E. Du, Q. Feng, C. D. Chen, Y. Tanaka, and X. J. Yang, Photocatalytic and dye-sensitized solar cell performances of {010}-faceted and [111]-faceted anatase TiO_2 nanocrystals synthesized from tetratitanate nanoribbons, *ACS App. Mater. Interfaces*, 2014, **6**, 16007-16019.

19 Y.-E. Du, D. J. Du, Q. Feng, and X. J. Yang, Delithation, exfoliation and transformation of rock-salt-structured Li_2TiO_3 to highly exposed {010}-faceted anatase, *ACS App. Mater. Interfaces*, 2015, **7**, 7995-8004.

20 X. J. Feng, K. Shankar, O. K. Varghese, M. Paulose, T. J. Latempa, and C. A. Grimes, Vertically aligned single crystal TiO_2 nanowire arrays grown directly on transparent conducting oxide coated glass: synthesis details and applications, *Nano Lett.*, 2008, **8**, 3781-3786.

21 P. P. Sun, X. T. Zhang, X. P. Liu, L. L. Wang, C. H. Wang, J. K. Yang, and Y. C. Liu, Growth of single-crystalline rutile TiO_2 nanowire on titanate nanosheet film for dye-sensitized solar cells, *J. Mater. Chem.*, 2012, **22**, 6389-6393.

22 X. L. Liu, H. M. Zhang, X. D. Yao, T. C. An, P. R. Liu, Wang, Y. F. Peng, A. R. Carroll, and H. J. Zhao, Visible light active pure rutile TiO_2 photoanodes with 100% exposed pyramid-shaped surfaces, *Nano Res.*, 2012, **5**, 762-769.

23 L. B. Yu, Z. Li, Y. B. Liu, F. Cheng, and S. Q. Sun, Synthesis of hierarchical TiO_2 flower-rod and application in CdSe/CdS co-sensitized solar cell, *J. Power Sources*, 2014, **270**, 42-52.

24 H. Wang, G. B. Yi, M. Tan, X. H. Zu, H. S. Luo, and X. M. Jiang, Initial reactant controlled synthesis of double layered TiO_2 nanostructure and characterization of its spectra of absorption and photoluminescence, *Mater. Lett.*, 2015, **148**, 5-8.

25 H. Izawa, S. Kikkawa, and M. Koizumi, Ion exchange and dehydration of layered titanate, $Na_2Ti_3O_7$ and $K_2Ti_4O_9$, *J. Phys. Chem.*, 1982, **86**, 5023-5026.

26 P. Maireles-Torres, P. Olivera-Pastor, E. Rodriguez-Castellon, A. Jimenez-Lopez, L. Alagna, and A. A. G. Tomlinson, Porous cross-linked materials formed by

oligometric aluminium hydroxide and α-Tin phosphate, *J. Mater. Chem.* 1991, **1**, 319-326.

27 S. Cheng, and T. Wang, Pillaring of layered titanates by polyoxo cations of aluminum, *Inorg. Chem.*, 1989, **28**, 1283-1289.

28 X. K. Li, B. Yue, and J. H. Ye, Photocatalytic hydrogen evolution over SiO_2-pillared and nitrogen-doped titanic acid under visible light irradiation, *Appl. Catal., A* 2010, **390**, 195-200.

29 W. H. Hou, Y. S. Chen, C. X. Guo, and Q. J. Yan, Synthesis of porous chromia-pillared tetratitanate, *J. Solid State Chem.*, 1998, **136**, 320-321.

30 S. Suzuki, and M. Miyayama, Lithium intercalation properties of octatitanate synthesized through exfoliation/reassembly, *J. Phys. Chem. B*, 2006, 110, 4731-4734.

31 H. Z. Zhang, and J. F. Banfield, Understanding polymorphic phase transformation behavior during growth of nanocrystalline aggregates: insights from TiO_2, *J. Phys. Chem. B*, 2000, **104**, 3481-3487.

32 J.-G. Yu, J. C. Yu, B. Cheng, S. K. Hark, and K. Iu, The effect of F^--doping and temperature on the structural and textural evolution of mesoporous TiO_2 powders, *J. Solid State Chem.*, 2003, **174**, 372-380.

33 F. Zuo, R. J. Dillon, L. Wang, P. Smith, X. Zhao, C.Bardeen, and P. Feng, Active facets on titanium (III)-doped TiO_2: a effective strategy to improve the visible-light photoctalytic, *Angw. Chem.Int. Ed.*, 2012, **51**, 6223-6226.

34 T. Gomez, X. Zarate, E. Schott, and R. Arratia-Perez, Role of the main adsorption modes in the interaction of the dye [COOH-TPP-Zn(II)] on a periodic TiO_2 slab exposing a rutile (110) surface in a dye-sensitized solar cell, *RSC Adv.*, 2014, **4**, 9639-9646.

35 J. N. Clifford, E. Martíez-Ferrero, A. Viterisi, and E. Palomares, Sensitizer molecular structure-device efficiency relationship in dye sensitized solar cells, *Chem. Soc. Rev.*, 2011, **40**, 1635-1646.

36 C. Y. Zha, L. M. Shen, X. Y. Zhang, Y. F. Wang, B. A. Korgel, A. Gupta and N. Z. Bao, Double-sided brush-shaped TiO_2 nanostructure assemblies with highly ordered nanowires for dye-sensitized solar cells, *ACS Appl. Mater. Interfaces*, 2014, **6**, 122-129.

37 Y. C. Rui, Y. G. Li, H. Z. Wang, and Q. H. Zhang, Photoanode Based on chain –shaped anatase TiO_2 nanorods for high-efficiency dye-sensitized solar cells, *Chem. Asian J.*, 2012, **7**, 2313-2320.

38 P. Wen, M. Xue, Y. Ishikawa, H. Itoh, and O. Feng, Relationships between cell parameters of dye-sensitized solar cells and dye-adsorption parameters, *ACS Appl. Mater. Interfaces*, 2012, **4**, 1928-2934.

39 U. Diebold, The surface science of titanium dioxide, *Surf. Sci. Rep.*, 2003, **48**, 53-229.

40 M. Ramamoorthy, D. Vanderbilt, and R. D. King-Smith, First-principles calculation of the energetic of stoichiometric TiO_2 surfaces, *Phys. Rev. B* 1994, **49**, 16721-16727.

41 J. Pan, G. Liu, G. Q. Lu, and H.-M. Cheng, On the true photoreactivity order of {001}, {010}, and {101} facets of anatase TiO_2 crystals, *Angew. Chem. Int. Ed.*, 2011, **50**, 2133-2137.